RSC Advances

ROYAL SOCIETY OF CHEMISTRY

PAPER

View Article Online
View Journal | View Issue

Check for updates

Cite this: *RSC Adv.*, 2020, **10**, 21019

Magnetic ion oxidation state dependent magnetoelectric coupling strength in Fe doped BCT ceramics

Aanchal Chawla,[a] Anupinder Singh,[a] P. D. Babu[b] and Mandeep Singh *[a]

Received 1st February 2020
Accepted 20th May 2020

DOI: 10.1039/d0ra00969e

rsc.li/rsc-advances

Polycrystalline samples of $Ba_{0.96}Ca_{0.04}Ti_{0.91}Fe_{0.09}O_3$ were prepared using a conventional solid state reaction route with different Fe starting precursors (Fe_2O_3, Fe_3O_4). The Rietveld refined XRD data confirmed the phase purity and tetragonal crystal structure of both the samples. The average grain size measured using SEM was ≈0.40 μm in both the samples. XPS analysis confirmed the presence of only Fe^{2+} and both Fe^{2+}/Fe^{3+} in Fe_2O_3 and Fe_3O_4 doped BCT samples. The P_r and M_r values have been measured to be 1.34 μC cm^{-2}, 2.88 μC cm^{-2} and 0.0015 emu g^{-1} and 0.135 emu g^{-1} in Fe_2O_3 and Fe_3O_4 doped BCT samples, respectively. The Fe_3O_4 doped samples exhibit much better M-E coupling (≈22%) as compared to Fe_2O_3 (≈7%) doped BCT samples. The results obtained hence suggest that Fe_3O_4 doping in BCT is better suited for multiferroic applications.

1 Introduction

In the past few decades, multiferroic materials having multiple coexisting ferroic properties (ferroelectricity, anti/ferromagnetism *etc*) have been extensively researched. The research in this field is still being extensively pursued. These materials have potential applications in fields like data storage, multiple-state memory devices and spintronics.[1–3] The interaction between different ferroic orders may allow the control of magnetic/electric polarization using external electric/magnetic fields. This coupling between different ferroic orders is of great potential for various practical applications especially in the field of spintronics, low energy consumption and memory devices.[4–7] However, naturally occurring multiferroic materials are rare. Therefore practically these multiferroic materials are fabricated by (a) doping of magnetic ions in otherwise ferroelectric material or (b) by making a composite of a ferromagnetic and a ferroelectric material.[8] Among a number of magnetic ion doped multiferroic materials, lead based perovskite materials have drawn considerable attention due to their high dielectric and piezoelectric coefficients. However, due to toxic nature of lead based compounds, research is being increasingly focussed to synthesize environment friendly alternatives like $BiFeO_3$, $TbMnO_3$ and $BaTiO_3$ based single phased multiferroic materials.[9]

$BaTiO_3$ (BT) which also has perovskite structure is a potential alternative for lead free multiferroics. BT and BT-based solid solutions exhibit large piezoelectric response, have high dielectric constant and thus find utility in almost all the aforementioned technologies. The experimental and theoretical studies both support the feasibility of multiferroicity in transition metal (Mn, Fe, Cr, *etc*) doped BT.[10–16] Effect of transition metal doping in BT is well documented in the literature. However, it has been observed that small amount of transition metal (TM) doping in BT results in a change in crystal structure from tetragonal to hexagonal (non-ferroelectric). Ca substituted BT (BCT) has been reported to inhibit the hexagonal phase formation. Additionally, it also helps to broaden the temperature dependence of the dielectric constant and provide large piezoelectric response, thus significantly enhancing the performance of BT based ceramics.[16,17] However, investigations on multiferroicity in magnetic ion doped BCT are very limited. Keswani *et al.*[18] reported the multiferroic properties of $Ba_{0.92}Ca_{0.08}Ti_{(1-x)}Fe_xO_3$ with Fe content varying from 0–5 wt% (sintered at 1240 °C for 5 h). They reported phase transformation into orthorhombic structure at 5% Fe concentration. They reported their best room temperature P_r, M_s and H_c values to be 2.13 μC cm^{-2}, 1.2175 emu g^{-1} and 13.11 Oe in 5% Fe substituted samples. Sharma *et al.*[19] reported the multiferroic properties $Ba_{0.92}Ca_{0.08}Ti_{(1-3x/4)}Fe_xO_3$ for x varying from 0.00 to 0.02 (in samples sintered at 1350 °C for 4 h). They reported an increase in P_r from 7.295 μC cm^{-2} to 9.359 μC cm^{-2} as x varies from 0.00 to 0.02. However, the magnetic results were not that encouraging. Moreover, the coupling between magnetic and ferroelectric orders has not yet been explored in these systems. Thus, Fe doped BCT ceramic needs to be explored further for improvement in multiferroic properties. Since the oxidation state of magnetic ions greatly impacts the multiferroic properties of the ceramic samples, it is hence crucial to compare the

---

[a] *Material Science and Characterization Laboratory, Department of Physics, Guru Nanak Dev University, Amritsar, Punjab 143005, India. E-mail: jmskhalsa@gmail.com*
[b] *UGC-DAE Consortium for Scientific Research, R-5 Shed, BARC, Mumbai, 400085, India*

multiferroic properties of magnetic ion doped BCT samples in which the same magnetic ion is in different oxidation states. In this regards, we report synthesis of Fe doped BCT samples using Fe_3O_4 and Fe_2O_3 (Fe = 0.09 wt%) magnetic ion precursors. The structural, microstructural, ferroelectric and magnetic properties have been analysed in detail. From the application point of view, magneto-PE measurements have also been reported.

2 Experimental procedure

$Ba_{0.96}Ca_{0.04}Ti_{0.91}Fe_{0.09}O_3$ ceramics were synthesised using conventional solid state reaction route method using Fe_2O_3 (named BCTF2) and Fe_3O_4 (BCTF3) as different Fe starting precursors. The stoichiometrically weighed raw materials ($BaCO_3$, $CaCO_3$, TiO_2, Fe_3O_4 and Fe_2O_3 (99.9% from pure Sigma Aldrich)) were ball milled for 48 h in acetone medium and calcined at 1000 °C for 12 hours. The PVA (2 wt%) was added to the calcined powders for pellet formation (1 mm thickness and 10 mm diameter). The pellets were then sintered at 1260 °C for 3 hours.

The XRD data was recorded using SHIMADZU (MAXima XRD-7000) equipped with CuKα anode ($\lambda = 1.5405$ Å). FESEM micrographs were recorded using Carl Zeiss "Supra 55" operating at 10 kV. Automatic ferroelectric loop tracer (from Marine India) was used for *P–E* measurements (at 50 Hz). The magnetic measurements were carried out using Vibrating Sample Magnetometer (VSM) EZ9 from Microsense and Quantum Design made PPMS. The X-ray Photoelectron Spectra (XPS) data was measured using Thermofisher scientific (Model-Nexsa base).

2.1. Microstructural characterizations

The raw and refined XRD diffractograms of BCTF2 and BCTF3 samples are shown in Fig. 1a and b. The samples are well crystallised as is indicated by the presence of sharp and high intensity diffraction peaks. The signature splitting of the diffraction peak at $2\theta \approx 45°$ provides initial evidence of the tetragonal structure of these samples. A comparative analysis of experimental and reference data (ICSD 98-000-3900) reveals that all the diffraction peaks can be assigned to a single tetragonal unit cell (space group *P4mm*). No secondary phase could be detected in both the samples. Rietveld analysis of the diffraction data was further carried out using Fullprof Suite 2015 software to determine various structural parameters of these samples.[20] The initial structural model for carrying out Rietveld refinement was assumed to be same as given in the reference data file ICSD 98-000-3900, for both the samples. The Ba/Ca, Ti/Fe, O1 and O2 were placed at the Wyckoff sites 1*a* (0, 0, 0), 1*b* (1/2, 1/2, 1/2 ± *δz*), 1*b* (1/2, 1/2, 0 ± *δz*) and 2c (1/2, 0, 1/2 ± *δz*), respectively. Here, *δ* indicates that the position co-ordinate is to be refined. The '*z*' coordinate was thus kept fixed for Ba/Ca while it was refined for Ti/Fe, O1 and O2. The lattice parameters of the selected phase and isotropic thermal parameters for various elements were also refined. The site occupancy parameters of various elements were set according to the stoichiometric calculation and were not refined. Peak profile and the background were modelled using a Thomson–Cox–Hasting pseudo-Voigt function and a sixth order polynomial, respectively. All the refinable parameters were successively refined (one at a time) till the discrepancy factors got minimised. The structural, discrepancy and other parameters obtained at the end of the refinement process have been listed in Table 1. The table clearly shows a GOF value of 1.28 and 1.31 for BCTF2 and BCTF3 samples, respectively. The very low values of GOF indicate a very good match between experimental data and the data generated using the structural model. The low GOF values hence validate the correctness of the initial structural model for both the samples. Further, the lattice parameters of both the samples are nearly same. This was expected because both the samples were substituted with Fe precursors having different Fe oxidation states only. The *c*/*a* ratio was hence found to be ≈1.005 in both the samples. In contrast to the reported transition from tetragonal to orthorhombic phase in $Ba_{0.92}Ca_{0.08}Ti_{(1-x)}Fe_xO_3$ system ($x = 0.05$, sintered at 1240 °C for 5 h) by Keswani *et al.*, we do not observe any such transition. The system continues to be in tetragonal phase up to $x = 0.09$ (sintered at 1260 °C for 3 h). As there is no significant difference in sintering temperature, the phase transition observed by Keswani *et al.*[18] might be due to higher Ca substitution (8%) as compared to 4% Ca substitution in our samples.

The Fig. 2a and b shows the FESEM images of BCTF2 and BCTF3 samples recorded at 30k×. Both the samples show the presence of a single type, small sized, isolated as well as agglomerated and random shaped grains. These samples also exhibit porosity as is evident by the presence of number of voids. The average grain size (calculated using Image J software) of BCTF2 and BCTF3 samples is ≈0.38 μm and 0.42 μm, respectively. The statistical distribution of grain size in both the samples is shown as histogram in Fig. 2.

In order to determine the impact of different starting precursors on the oxidation state of Fe in BCTF2 & BCTF3 samples, XPS analysis was carried out. The XPS core level spectra were collected from the surface of the samples for all the elements. However, only Fe core level spectra are shown in Fig. 3a and b as the magnetic and ferroelectric properties of these samples are dependent upon the oxidation state of Fe. The deconvolution (in the 703–719 eV range) was hence carried out accordingly. The peak at lower binding energy has been associated to Fe^{2+} oxidation state in compliance with literature.[21] This peak is present in the both the samples. An additional peak corresponds to Fe^{3+} is only present in BCTF3 samples. A shake up satellite peak was observed in both the samples. The peaks have been duly marked in Fig. 3. The XPS analysis hence confirms the presence of only Fe^{2+} ions in BCTF2 sample and Fe^{2+}, Fe^{3+} ions in BCTF3 sample. The relative concentration of Fe^{2+} and Fe^{3+} (from area under the peak) in BCTF3 sample was found out to be nearly 1 : 1.64. As per charge balancing requirements, presence of Fe^{2+} states only is expected to result in higher concentration of oxygen vacancies as compared to simultaneous presence of Fe^{2+} and Fe^{3+}. As oxygen vacancies contribute to the flow of leakage current, the BCTF2 sample is expected to have higher conductivity (hence lower P_r) as compared to BCTF3 sample. This is also observed (also to be

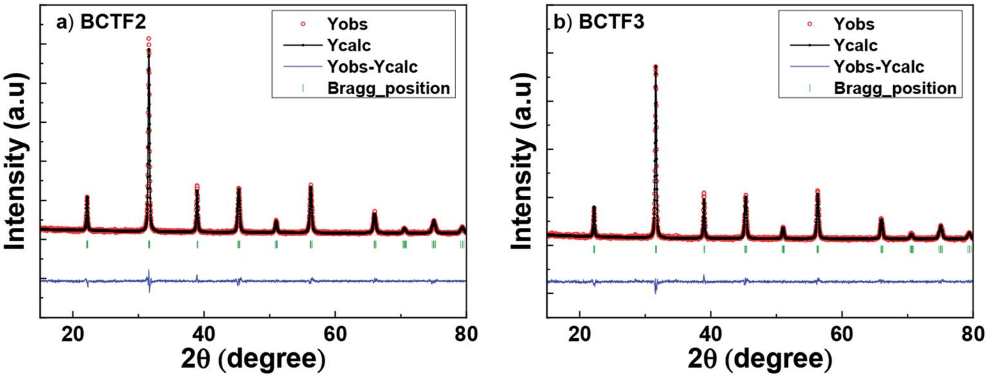

Fig. 1 -The raw and Rietveld refined XRD data of (a) BCTF2 and (b) BCTF3 samples, respectively.

discussed in ferroelectric properties section). As BCTF3 sample shows simultaneous presence of multivalent Fe states, the magnetic properties of BCTF3 sample are also expected to be better than BCTF2 samples because of enhanced contribution of double exchange. The observed difference in the XPS spectra of these two samples might be due to the difference in the melting points of Fe_2O_3 (1565 °C) and Fe_3O_4 (1597 °C).[22] As we sintered these samples at 1260 °C, further oxidation (to Fe^{4+}) is hence not expected. Keswani *et al.* reported the presence of only Fe^{3+} (≈709.76) in Fe_2O_3 doped BCT samples sintered at 1240 °C for five hours.[18] Guo *et al.* reported the presence of Fe^{3+} (≈710.7 eV), Fe^{4+} (≈712.6 eV) and a satellite peak at 718.4 eV in Fe_3O_4 doped BT samples sintered at 1223 °C for 24 hours.[23] However, in our samples (sintered at 1260 °C for three hours) we observed peaks at ≈708.9 eV, 710.6 eV and a broad peak at 714.5 eV (in BCTF3 sample) which we associated with Fe^{2+}, Fe^{3+} and combined satellite peak corresponding to Fe^{2+} and Fe^{3+} in accordance with XPS handbook.[21] Note that we and Guo *et al.* observe Fe^{3+} peak at ≈710.6 eV.

2.2. Ferroelectric properties

The room temperature P–E loops of the BCTF2 and BCTF3 samples are shown in Fig. 4. It is clear from the figure that BCTF3 sample exhibits better ferroelectric behaviour as compared to the BCTF2 sample. None of the samples exhibits 'square' P–E loops which are expected in ferroelectric materials in which electric dipoles exhibit abrupt reversal of orientation with change in the direction of applied electric field. The roundish shape of P–E loops (more in BCTF2) of these samples indicates a sluggish response of their electric dipoles to external electric field.[24] The measured remnant polarisation ($P_{\downarrow}$(r)) values are 1.34 μC cm^{-2} and 2.88 μC cm^{-2} for BCTF2 and BCTF3 samples, respectively. The electric polarization in a given material generally varies with factors such as c/a ratio, grain size and flow of leakage current. The P_r values of both these samples (c/a ≈ 1.005) are smaller in comparison to the pure $BaTiO_3$ (c/a = 1.01, ref.). This can be directly attributed primarily to smaller tetragonal distortion (c/a ≈ 1.005) of our samples as compared to $BaTiO_3$ (BT). Also, Fe is known to enhance leakage current[1,25,26] when substituted in ferroelectrics. This can also be additionally responsible for lower observed P_r as compared to BT. However, among the BCTF2 and BCTF3 samples, BCTF2 exhibits lower P_r. Both of these samples have got equivalent c/a ratio (≈1.005), similar grain size (≈0.40 μm) and have equal Fe concentration. Thus, the variation of P_r in these samples is not associated with c/a ratio and grain size. This may rather be due to creation of a greater number of oxygen vacancies when Fe^{2+} replaces Ti^{4+} in BCTF2 sample as compared to Fe^{2+} and Fe^{3+} in BCTF3 sample as confirmed by XPS studies. It should be noted that the BCTF3 sample has lower room temperature dc conductivity (1.59 × 10^{-6} S cm^{-1}) as compared to BCTF2 sample (4.23 × 10^{-5} S cm^{-1}), implying lower value of leakage current (hence higher P_r) in BCTF3 sample. Thus, higher conductivity of BCTF2 sample precludes the measurement of P_r

Table 1 The lattice parameters, agreement indices of BCTF2 and BCTF3 samples obtained from Rietveld refinement

Sample	Cell parameter (Å)	Position coordinates				B_{iso}	R-Factors
		Atom sites	X	Y	Z		
BCTF2	$a = 3.99$	Ba/Ca	0.000	0.000	0.000	0.581	$R_p = 6.01$
	$c = 4.01$	Ti/Fe	0.500	0.500	0.518	0.722	$R_{wp} = 7.59$
	$c/a = 1.005$	O1	0.000	0.500	0.471	0.626	$R_{exp} = 6.67$
		O2	0.500	0.500	0.971	0.777	GOF = 1.29
BCTF3	$a = 3.99$	Ba/Ca	0.000	0.000	0.000	0.655	$R_p = 6.46$
	$c = 4.01$	Ti/Fe	0.500	0.500	0.520	0.571	$R_{wp} = 8.11$
	$c/a = 1.005$	O1	0.000	0.500	0.465	0.834	$R_{exp} = 7.12$
		O2	0.500	0.500	0.965	0.789	GOF = 1.30

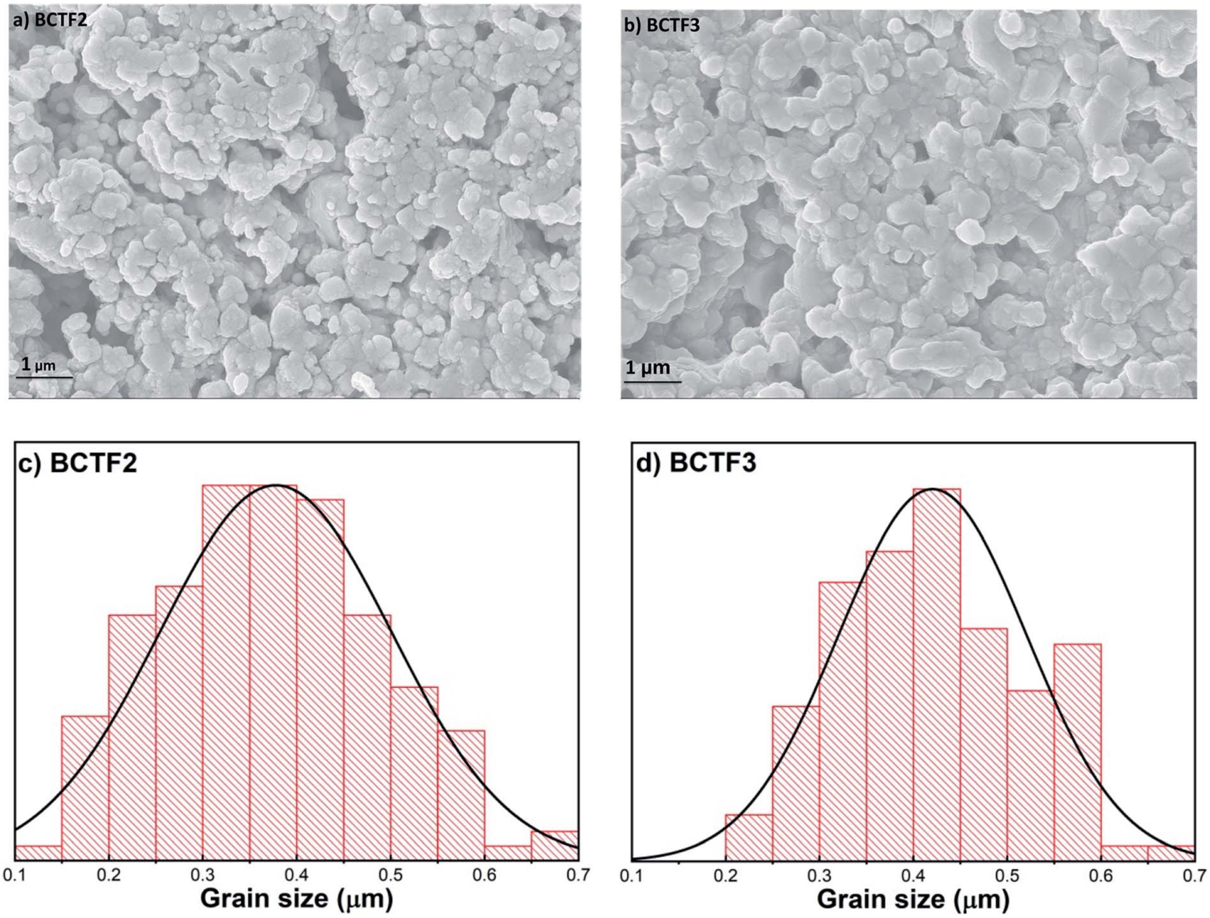

Fig. 2 The SEM micrographs of (a) BCTF2, (b) BCTF3 and statistical distribution of grain size of (c) BCTF2 and (d) BCTF3 samples, respectively.

as compared to the BCTF3 sample. Additionally, contribution to P_r in BCTF3 sample can come from ferroelectricity driven by charge ordering due to simultaneous presence of both Fe^{2+} and Fe^{3+} oxidation states in this sample.[27,28] The presence of multivalent Fe states leads to electron trapping between the two Fe sites. This trapped electron ends up creating double exchange as well as polaronic-type distortion which act together to form a vibrionic localized electronic state. This vibrionic state results in bond centred type charge ordering which is also known as Zenor polaron state.[29] The ferroelectricity driven by charge ordering has already been reported in a number of materials such as $Pr_{1-x}Ca_xMnO_3$, $LuFe_2O_4$ *etc.*[27] The increase in P_r value with Fe substitution have already been reported in BCT system. However, our BCTF3 sample exhibit better ferroelectric properties and higher P_r value as compared to the value reported by Keswani *et al.*[18] even at 9% Fe substitution. However, the higher

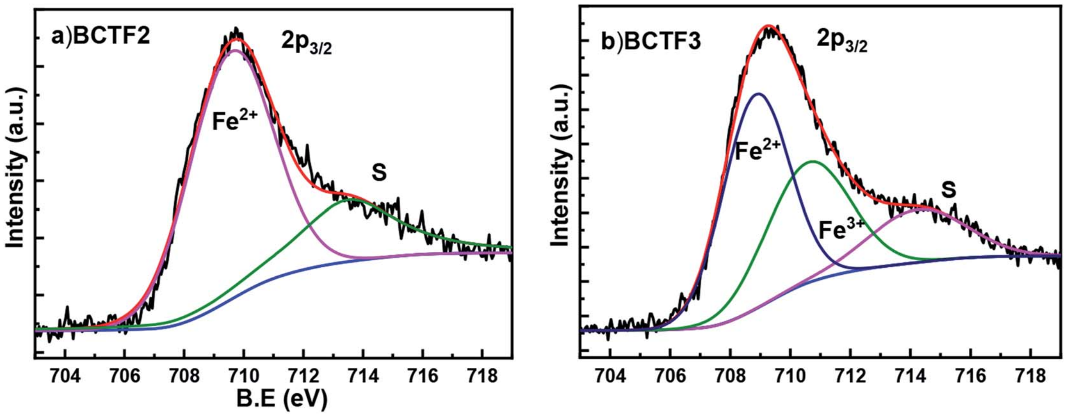

Fig. 3 The deconvoluted $2p_{3/2}$ spectrum of Fe in (a) BCTF2 and (b) BCTF3 samples, respectively.

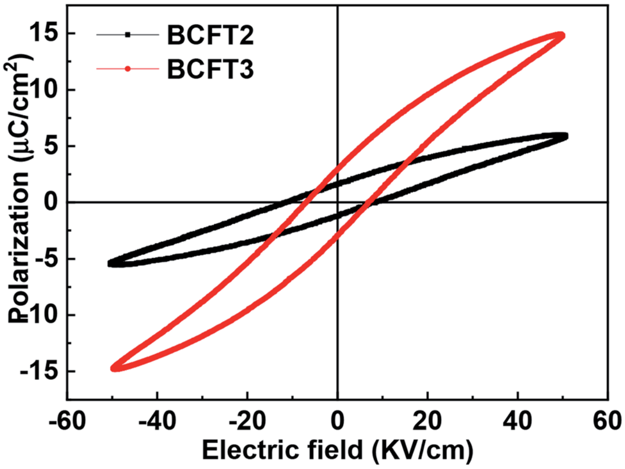

Fig. 4 The room temperature P–E loops of BCTF2 and BCTF3 samples, respectively.

P_r value reported by Sharma *et al.*[19] may be due to higher sintering temperature (1350 °C) and lower Fe concentration.

2.3. Magnetic properties

The room temperature M–H plots of the BCTF2 and BCTF3 samples are shown in Fig. 5a and b. The graphs elucidates that both the sample exhibit magnetic behaviour. However, the BCTF3 sample displays better magnetic behaviour as is indicated by its clearer hysteresis loop as compared to the BCTF2 sample. The magnetization of BCTF2 sample displays almost linear behaviour in the higher magnetic field region where as the magnetization of the BCTF3 sample appears to approach a certain saturation value. This is again indicative of the strong nature of magnetic ordering in the BCTF3 sample as compared to BCTF2 sample. The room temperature remnant magnetization (M_r) was observed to be 0.0015 emu g^{-1} and 0.135 emu g^{-1} for the BCTF2 and BCTF3 samples, respectively. As per Goodenough–Kanamori rules, half-filled (*e.g.* Fe^{3+}) and more than half filled (*e.g.* Fe^{2+}) transition metal d-orbitals favour antiferromagnetic super exchange interaction between two Fe ions *via* oxygen anion.[30] Also, recall that, the XPS data had shown the presence of Fe^{2+} only and both Fe^{2+} and Fe^{3+} ions in BCTF2 and BCTF3 samples. The Fe doping level used in the present case is equivalent to what are typically used in dilute magnetic semiconductors (DMS). In DMS and dilute magnetic oxide systems, the magnetic interactions are generally described using either Zener model[31] or RKKY interactions.[32] For these mechanisms to be dominant, the material must have high electrical conductivity ($\approx 20 \times 10^{-3}$ S cm^{-1}) and hence high free carrier concentration.[33–39] Please note that the conductivity of BCTF3 and BCTF2 samples is $\approx 1.59 \times 10^{-6}$ S cm^{-1} and 4.23×10^{-5} S cm^{-1}. The T_c values reported in various high carrier density DMS system's are generally ≤300 K. Thus, RKKY interaction does not seem to be the feasible mechanism because of lower electrical conductivity and high T_c ($\approx$650 K) of our samples. Dugaev *et al.* also proposed a mechanism of ferromagnetism in DMS at low charge density.[40] However, this mechanism also predicts T_c values ≈ 100 K and is therefore

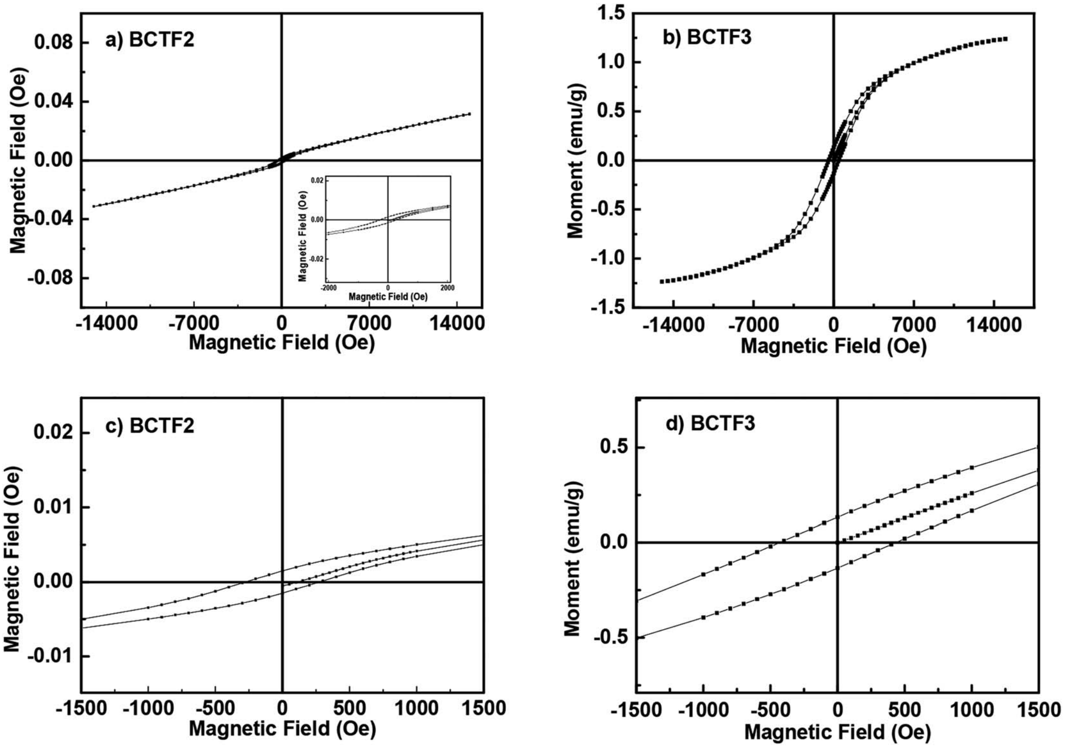

Fig. 5 The room temperature M–H plots of (a) BCTF2, (b) BCTF3 samples and magnified M–H plots (c) BCTF2 and (d) BCTF3 samples, respectively.

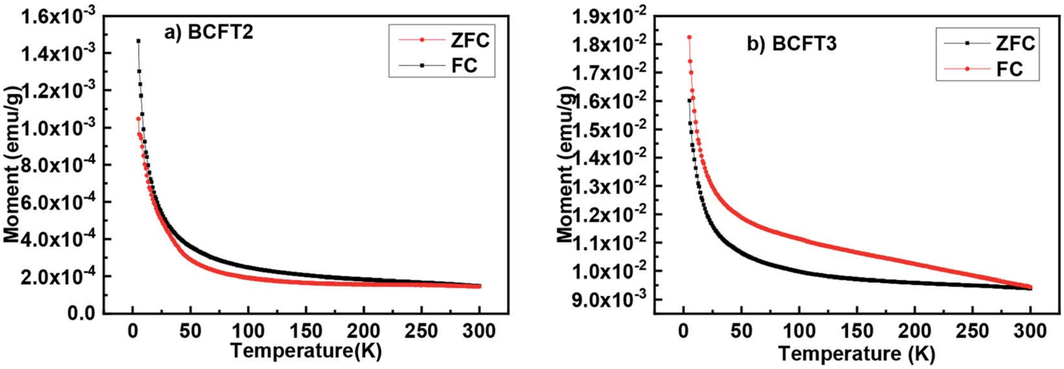

Fig. 6 The low temperature ZFC/FC data of (a) BCTF2 and (b) BCTF3 samples, respectively.

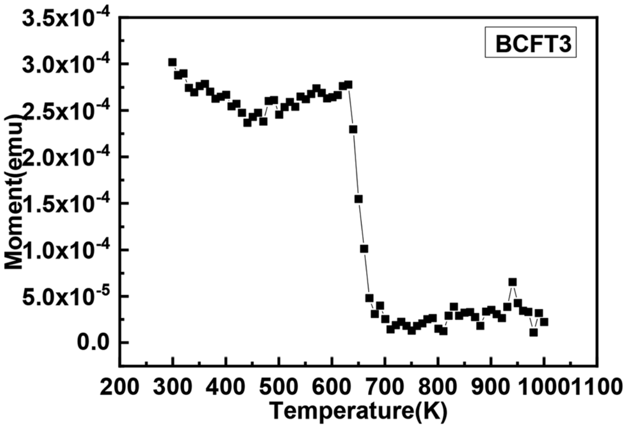

Fig. 7 The high temperature *M vs. T* data of BCTF3 sample.

ruled out. Coey *et al.* proposed another model (generally referred to as DIBE model) for dilute ferromagnetic oxides having T_c much larger than 300 K.[41] The model is applicable to systems which have transition metal (TM) dopant concentration lower than the percolation threshold and the saturation magnetic moment per TM ion is greater than the spin only moment. As per Coey, in such systems, (a) super-exchange cannot be invoked, (b) rarely does superexchange systems have net moment per TM ion greater than 1 μ_B, and (c) though double exchange can in principle produce large moments but mixed valence (which is central to existence of double exchange) is not a common feature of such dilute systems. The saturation moment per Fe ion in our BCTF2 and BCTF3 samples have been determined to be $\approx 0.02\ \mu_B$ and 0.61 μ_B. Also, the percolation threshold values for Fe^{2+} and Fe^{2+}/Fe^{3+} (40 : 60 ratio) doping in BCT have been calculated to be ≈5.15 at% and 6.76 at%. Note that, (a) the saturation moments observed in our samples are much lower than spin only moments, (b) the doping level is above the percolation threshold and (c) we are observing multiple Fe states in BCTF3 sample. Hence, these arguments rule out the applicability of DIBE model and favour the presence of superexchange and double exchange in our respective samples. F-centre exchange (FCM) is also invoked in literature to explain strong ferromagnetism and high T_c in TM doped oxide systems (above percolation threshold).[42] This mechanism relies on indirect exchange between two Fe^{3+} ions *via* electron trapped at oxygen vacancy site. Clearly this does not seem to be a feasible mechanism in our case owing to weak magnetic behaviour of BCTF2 sample and multiple Fe states in BCTF3 sample. Hence, in view of the discussions presented above we believe that super exchange and double exchange to be the mechanisms responsible for the observed magnetic behaviour of BCTF2 and BCTF3 samples. It should be noted that Guo *et al.* invoked double exchange between Fe^{3+}/Fe^{4+} ions in Fe doped BT (Fe varying from 10–60 at%). However, (a) they have used very

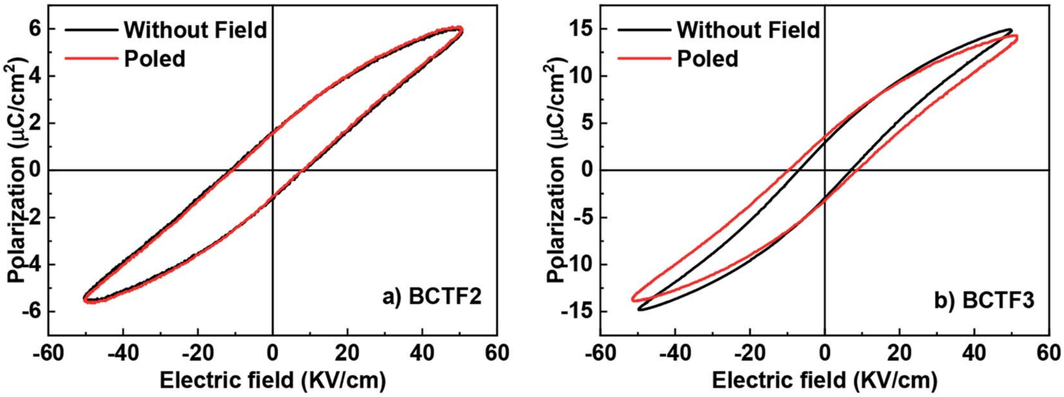

Fig. 8 The room temperature without field and poled *P–E* loops of (a) BCTF2 and (b) BCTF3 samples, respectively.

Table 2 The unpoled, poled remnant polarization values and calculated *ME* coupling strength of BCTF2 and BCTF3 samples

Sample	Unpoled remnant polarization ($P_r(0)$) (μC cm^{-2})	Poled remnant polarization ($P_r(H)$) (μC cm^{-2})	*ME* strength
BCTF2	1.34	1.43	6.71%
BCTF3	2.88	3.51	21.8%

high Fe doping concentration and (b) reported the presence of Fe_3O_4 impurity phase (≈0.5 mol%) at high Fe concentrations. The double exchange interaction is well reported in oxide systems such as Fe_3O_4 in which mixed oxidation state exists.[43–45] In order to further study the nature of magnetic ordering in these samples, zero field cooled and field cooled (ZFC/FC) measurements were carried out. The ZFC/FC curves (below room temperature) of both the samples are shown in Fig. 6a and b. No discontinuity or inflection point is observed in the *M*–*T* data in this range. This clearly indicates (a) the absence of magnetic phase transition in both the samples in this temperature range and (b) that the samples exhibit a transition from magnetically ordered state to magnetically disordered state well above the room temperature. Further, the low temperature ZFC/FC curves do not superimpose each other and exhibit bifurcation at a temperature which is usually referred to as irreversibility temperature (T_{irr}). The T_{irr} has been observed to be ≈200 K and ≈300 K in BCTF2 and BCTF3 samples, respectively. It should be noted that non-superimposition of ZFC/FC curves is reported in a number of systems.[46–52] The non-superimposition of ZFC/FC curves is usually attributed to (a) coexistence of ferromagnetic and antiferromagnetic phases caused by magnetic frustration, (b) dominating effect of magnetic anisotropy and (c) spin glass behaviour.[53–56] In our samples, we believe that the divergence of ZFC and FC curves is most likely to be due to the spin glass behaviour. Further, the non-overlapping of ZFC/FC data in both the samples suggest that there is no true long range magnetic order. This type of behaviour is well reported in number of magnetically doped bulk and thin film perovskites such as $SrTiFeO_3$, $BaTiFeO_3$, $BaTiCoO_3$ and $BaZrFeO_3$.[43] Further, the magnetization *vs.* temperature (*M*–*T*) analysis were carried out in high temperature range (330 K–1000 K) for BCTF3 sample and is shown in Fig. 7. The graph clearly shows the magnetic transition at ≈650 K. The transition temperature observed in our sample is lower than the transition temperature reported for Fe_3O_4 (850 K) and Fe_2O_3 (1000 K).[13] This clearly rules out the possibility of presence of Fe_3O_4 and Fe_2O_3 clusters. Hence the magnetic properties of our sample (BCTF3) are intrinsic in nature and not due to the presence of impurity magnetic phases.

2.4. Magneto-electric properties

The investigation of coupling between the electric and magnetic orders in our samples was carried out by performing *P*–*E* measurements in the absence and presence of magnetic field. In this regard, the samples were first poled using a magnetic field strength of 1 T for 30 minutes. The *P*–*E* loops recorded in the absence (unpoled) and presence (poled) of magnetic field for BCTF2 and BCTF3 samples are shown in Fig. 8. It is clear from the graph that the poled and unpoled *P*–*E* loops of BCTF2 sample nearly overlap each other while the poled and unpoled *P*–*E* loops of BCTF3 sample shows a significant change. This indicates better *M*–*E* coupling in the BCTF3 sample as compared to BCTF2 sample. The values of P_r for both the samples have been listed in Table 2. The table clearly shows that the poled loops of the BCTF3 samples shows an enhancement in the P_r value. Higher P_r in case of poled samples indicates positive *M*–*E* coupling in both the samples. The strength of *M*–*E* coupling is generally measured as $[P_r(H) - P_r(0)/P_r(0)] \times 100$ where, $P_r(H)$ corresponds to P_r measured at 1 T after poling and $P_r(0)$ corresponds to P_r measured in the absence of magnetic field without poling. The strength of *M*–*E* coupling was found to be ≈21.8% and ≈6.71% in case of BCTF3 and BCTF2 samples, respectively. The *ME* coupling in these samples may be due to reorientation of spin magnetic moments by external magnetic field which induces strain in the material due to magnetostrictive effects. This strain in turn gets coupled with already existing ferroelectric order in the material thereby changing ferroelectric polarization.[4,6,7] The better *ME* response in the BCTF3 sample may be due to its better magnetic properties as compared to BCTF2 sample. Due to better magnetic properties of BCTF3 sample, magnetostrictive effects are stronger which in turn have further stronger effect on already existing ferroelectric orders.

3 Conclusion

$Ba_{0.96}Ca_{0.04}Ti_{0.91}Fe_{0.09}O_3$ samples were successfully prepared using solid state reaction route using different starting Fe precursors (Fe_2O_3, Fe_3O_4). The XRD analysis shows that both the samples crystallize in tetragonal structure with no additional impurity phase. No significant change in the either surface morphology or grain size has been observed with change in precursor material. The XPS analysis confirmed the presence of Fe in multiple oxidation states in BCTF3 sample. Better ferroelectric properties of BCTF3 sample have been attributed to electron trapping in different Fe states which results in bond centered charge ordering thereby enhancing ferroelectric character. Weaker magnetic behavior of BCTF2 sample has been explained to be due to super exchange which results in antiferromagnetic coupling between Fe^{2+} ions. The better magnetic properties of BCTF3 sample are due to presence of multivalent Fe states which results in double exchange interaction. The better *ME* coupling in BCTF3 sample is due to presence of stronger magnetic interaction which promotes stronger magnetostrictive effects and hence better coupling with ferroelectric order.

Conflicts of interest

There are no conflicts to declare.

Acknowledgements

The authors gratefully acknowledge UGC, New Delhi (F.30-115/2015(BSR)) and UGC-BSR (Aanchal) for providing financial assistance. The authors also acknowledge Centre for Emerging Life Sciences, GNDU, Amritsar and Dr R. J. Choudhary, UGC-DAE consortium Indore for help in various characterisations.

References

1 N. A. Hill, Why Are There so Few Magnetic Ferroelectrics?, *J. Phys. Chem. B*, 2000, **104**, 6694–6709, DOI: 10.1021/jp000114x.

2 D. I. Khomskii, Multiferroics: different ways to combine magnetism and ferroelectricity, *J. Magn. Magn. Mater.*, 2006, **306**, 1–8.

3 C. Ederer and N. A. Spaldin, A new route to magnetic ferroelectrics, *Nat. Mater.*, 2004, **3**, 849–851.

4 P. Guzdek, The magnetostrictive and magnetoelectric characterization of Ni0.3Zn0.62Cu0.08Fe2O4–Pb(FeNb)0.5O3 laminated composite, *J. Magn. Magn. Mater.*, 2014, **349**, 219–223, DOI: 10.1016/J.JMMM.2013.08.064.

5 C. Ederer and N. A. Spaldin, Weak ferromagnetism and magnetoelectric coupling in bismuth ferrite, *Phys. Rev. B: Condens. Matter Mater. Phys.*, 2005, **71**, 1–4, DOI: 10.1103/PhysRevB.71.060401.

6 S. Lather, A. Gupta, J. Dalal, V. Verma, R. Tripathi and A. Ohlan, Effect of mechanical milling on structural, dielectric and magnetic properties of BaTiO3–Ni0. 5Co0. 5Fe2O4 multiferroic nanocomposites, *Ceram. Int.*, 2017, **43**, 3246–3251.

7 J. Shah and R. K. Kotnala, Induced magnetism and magnetoelectric coupling in ferroelectric BaTiO 3 by Cr-doping synthesized by a facile chemical route, *J. Mater. Chem. A*, 2013, **1**, 8601–8608.

8 N. V Dang, T. D. Thanh, L. V Hong, V. D. Lam and T.-L. Phan, Structural, optical and magnetic properties of polycrystalline BaTi1− xFexO3 ceramics, *J. Appl. Phys.*, 2011, **110**, 43914.

9 S. T. Lau, C. H. Cheng, S. H. Choy, D. M. Lin, K. W. Kwok, H. L. W. Chan, S. T. Lau, C. H. Cheng, S. H. Choy, D. M. Lin, K. W. Kwok and H. L. W. Chan, Lead-free ceramics for pyroelectric applications Lead-free ceramics for pyroelectric applications, *J. Appl. Phys.*, 2011, 104105, DOI: 10.1063/1.2927252.

10 L. Chen, H. Fan and S. Zhang, Investigation of MnO2-doped (Ba, Ca) TiO3 lead-free ceramics for high power piezoelectric applications, *J. Am. Ceram. Soc.*, 2017, **100**, 3568–3576.

11 S. Ray, P. Mahadevan, S. Mandal, S. R. Krishnakumar, C. S. Kuroda, T. Sasaki, T. Taniyama and M. Itoh, High temperature ferromagnetism in single crystalline dilute Fe-doped BaTiO3, *Phys. Rev. B*, 2008, **77**, 104416, DOI: 10.1103/PhysRevB.77.104416.

12 N. Jedrecy, H. J. Von Bardeleben, V. Badjeck, D. Demaille, D. Stanescu, H. Magnan and A. Barbier, Strong magnetoelectric coupling in multiferroic Co/BaTiO 3 thin films, *Phys. Rev. B*, 2013, **88**, 121409.

13 B. Deka, S. Ravi, A. Perumal and D. Pamu, Ferromagnetism and ferroelectricity in Fe doped BaTiO3, *Phys. B*, 2014, **448**, 204–206.

14 L. Yang, H. Qiu, L. Pan, Z. Guo, M. Xu, J. Yin and X. Zhao, Magnetic properties of BaTiO3 and BaTi1− xMxO3 (M= Co, Fe) nanocrystals by hydrothermal method, *J. Magn. Magn. Mater.*, 2014, **350**, 1–5.

15 Z. Guo, L. Pan, C. Bi, H. Qiu, X. Zhao, L. Yang and M. Y. Rafique, Structural and multiferroic properties of Fe-doped Ba0. 5Sr0. 5TiO3 solids, *J. Magn. Magn. Mater.*, 2013, **325**, 24–28.

16 P. Victor, R. Ranjith and S. B. Krupanidhi, Normal ferroelectric to relaxor behavior in laser ablated Ca-doped barium titanate thin films Normal ferroelectric to relaxor behavior in laser ablated Ca-doped barium titanate thin films, *J. Appl. Phys.*, 2017, 7702, DOI: 10.1063/1.1618914.

17 A. Chawla, S. Verma, S. Godara, G. R. Bhadu, A. Singh and M. Singh, Understanding Phase Segregation Using Rietveld Analysis and the Dielectric, Ferroelectric Properties of Ba(1−x)CaxTiO3 Solid Solutions, *J. Electron. Mater.*, 2020, DOI: 10.1007/s11664-020-08150-6.

18 B. C. Keswani, R. S. Devan, R. C. Kambale, A. R. James, S. Manandhar, Y. D. Kolekar and C. V Ramana, Correlation between structural, magnetic and ferroelectric properties of Fe-doped (Ba-Ca) TiO3 lead-free piezoelectric, *J. Alloys Compd.*, 2017, **712**, 320–333.

19 P. Sharma, P. Kumar, R. S. Kundu, N. Ahlawat and R. Punia, Enhancement in magnetic, piezoelectric and ferroelectric properties on substitution of titanium by iron in barium calcium titanate ceramics, *Ceram. Int.*, 2016, **42**(10), 12167–12171, DOI: 10.1016/j.ceramint.2016.04.152.

20 J. Rodriguez-Carvajal, Fullprof. 2k, Version 4.6 c–Mar 2002, *Phys. B*, 1993, **55**, 192.

21 J. F. Moulder, W. F. S., P. E. Sobo and K. D. Bomben, *Handbook of X-ray Photoelectron Spectroscopy*, 1st edn, Perkin-Elmer Corporation Physical Electronics Division, United States, 1992.

22 J. A. Kerr, *CRC Handbook of Chemistry and Physics*, ed D. R. Lide, 81st edn, 2000.

23 Z. Guo, L. Yang, H. Qiu, X. Zhan, J. Yin and L. Cao, Structural, magnetic and dielectric properties of Fe-doped BaTiO 3 solids, *Mod. Phys. Lett. B*, 2012, **26**, 1250056.

24 B. Jaffe, *Piezoelectric Ceramics*, Academic Press, 1st edn, 1971.

25 A. Chawla, A. Singh and M. Singh, Effect of decreasing Mg 2+ and Zr 4+ substitution on the structural, ferroelectric and magnetic properties of BF-PT solid solutions, *Mater. Today Commun.*, 2018, **14**, 47–52.

26 M. A. Khan, T. P. Comyn and A. J. Bell, Leakage mechanisms in bismuth ferrite-lead titanate thin films on Pt/Si substrates, *Appl. Phys. Lett.*, 2008, **92**, 72908.

27 J. Van Den Brink and D. I. Khomskii, Multiferroicity due to charge ordering, *J. Phys. Condens. Matter*, 2008, **20**, 434217.

28 K. Yamauchi, T. Fukushima and S. Picozzi, Ferroelectricity in multiferroic magnetite Fe 3 O 4 driven by noncentrosymmetric Fe 2+/Fe 3+ charge-ordering: first-principles study, *Phys. Rev. B*, 2009, **79**, 212404.

29 A. Daoud-Aladine, J. Rodriguez-Carvajal, L. Pinsard-Gaudart, M. T. Fernandez-Diaz and A. Revcolevschi, Zener polaron ordering in half-doped manganites, *Phys. Rev. Lett.*, 2002, **89**, 97205.

30 J. B. Goodenough, Theory of the role of covalence in the perovskite-type manganites [La, M (II)] Mn O 3, *Phys. Rev.*, 1955, **100**, 564.

31 T. Dietl, Origin of ferromagnetic response in diluted magnetic semiconductors and oxides, *J. Phys. Condens. Matter*, 2007, **19**, 165204.

32 A. Werpachowska and Z. Wilamowski, The RKKY coupling in diluted magnetic semiconductors, *ArXiv Prepr., ArXiv1111.1030*, 2011.

33 K. Gopinadhan, D. K. Pandya, S. C. Kashyap and S. Chaudhary, Cobalt-substituted Sn O_2 thin films: A transparent ferromagnetic semiconductor, *J. Appl. Phys.*, 2006, **99**, 126106.

34 K. Ueda, H. Tabata and T. Kawai, Magnetic and electric properties of transition-metal-doped ZnO films, *Appl. Phys. Lett.*, 2001, **79**, 988–990.

35 Y. Matsumoto, M. Murakami, T. Shono, T. Hasegawa, T. Fukumura, M. Kawasaki, P. Ahmet, T. Chikyow, S. Koshihara and H. Koinuma, Room-temperature ferromagnetism in transparent transition metal-doped titanium dioxide, *Science*, 2001, **291**, 854–856.

36 T. Fukumura, Z. Jin, M. Kawasaki, T. Shono and T. Hasegawa, Magnetic properties of Mn-doped ZnO, *Appl. Phys. Lett.*, 2001, **78**, 3824.

37 P. Sharma, A. Gupta, K. V Rao, F. J. Owens, R. Sharma, R. Ahuja, J. M. O. Guillen, B. Johansson and G. A. Gehring, Ferromagnetism above room temperature in bulk and transparent thin films of Mn-doped ZnO, *Nat. Mater.*, 2003, **2**, 673–677.

38 K. Gopinadhan, S. C. Kashyap, D. K. Pandya and S. Chaudhary, Evidence of carrier mediated room temperature ferromagnetism in transparent semiconducting Sn1 − *x*Co*x*O2 − *δ* thin films, *J. Phys. Condens. Matter*, 2008, **20**, 125208.

39 K. Gopinadhan, D. K. Pandya, S. C. Kashyap and S. Chaudhary, On the blueshift in Sn1 − *x*Co*x*O2 − δ transparent ferromagnetic semiconductor thin films, *J. Phys. Condens. Matter*, 2006, **19**, 16216.

40 V. K. Dugaev, V. I. Litvinov, J. Barnaś, A. H. Slobodskyy, W. Dobrowolski and M. Vieira, Mechanism of ferromagnetism in diluted magnetic semiconductors at low carrier density, *J. Supercond.*, 2003, **16**, 67–70.

41 J. M. D. Coey, *Donor Impurity Band Exchange in Dilute Ferromagnetic Oxides*, 2014, DOI: 10.1038/nmat1310.

42 J. M. D. Coey, A. P. Douvalis, C. B. Fitzgerald and M. Venkatesan, Ferromagnetism in Fe-doped SnO 2 thin films, *Appl. Phys. Lett.*, 2004, **84**, 1332–1334.

43 H.-S. Kim, L. Bi, G. F. Dionne and C. A. Ross, Magnetic and magneto-optical properties of Fe-doped Sr Ti O 3 films, *Appl. Phys. Lett.*, 2008, **93**, 92506.

44 P. P. Khirade, S. D. Birajdar, A. V Raut and K. M. Jadhav, Effect of Fe–substitution on phase transformation, optical, electrical and dielectrical properties of BaTiO 3 nanoceramics synthesized by sol-gel auto combustion method, *J. Electroceram.*, 2016, **37**, 110–120.

45 B. Deka, S. Ravi, A. Perumal and D. Pamu, Ferromagnetism and ferroelectricity in Fe doped $BaTiO_3$, *Phys. B*, 2014, **448**, 204–206.

46 P. A. Joy, P. S. A. Kumar and S. K. Date, The relationship between field-cooled and zero-field-cooled susceptibilities of some ordered magnetic systems, *J. Phys. Condens. Matter*, 1998, **10**, 11049.

47 J. E. Greedan, N. P. Raju, A. Maignan, C. Simon, J. S. Pedersen, A. M. Niraimathi, E. Gmelin and M. A. Subramanian, Frustrated pyrochlore oxides, Y 2 Mn 2 O 7, Ho 2 Mn 2 O 7, and Yb 2 Mn 2 O 7: bulk magnetism and magnetic microstructure, *Phys. Rev. B*, 1996, **54**, 7189.

48 A. Maignan, A. Sundaresan, U. V Varadaraju and B. Raveau, Magnetization relaxation and aging in spin-glass (La, Y) 1−xCaxMnO3 (x= 0.25, 0.3 and 0.5) perovskite, *J. Magn. Magn. Mater.*, 1998, **184**, 83–88.

49 A. Maignan, U. V Varadaraju, F. Millange and B. Raveau, AC susceptibilities and size effect in Ln0. 7 (Sr, Ca) 0.3 MnO3 CMR manganites, *J. Magn. Magn. Mater.*, 1997, **168**, L237–L242.

50 X. L. Wang, J. Horvat, H. K. Liu and S. X. Dou, Spin-glass state in Y0. 7Ca0. 3MnO3, *J. Magn. Magn. Mater.*, 1998, **182**, L1–L4.

51 J. Pérez, J. Garcia, J. Blasco and J. Stankiewicz, Spin-Glass Behavior and Giant Magnetoresistance in the (RE) Ni 0.3 Co 0.7 O 3 (R E= L a, N d, S m) System, *Phys. Rev. Lett.*, 1998, **80**, 2401.

52 I. O. Troyanchuk, N. V Samsonenko, E. F. Shapovalova, H. Szymczak and A. Nabialek, Synthesis and characterization of Ln (B0. 5Mn0. 5) O3 (Ln-lanthanoid; B= Ni, Co) perovskites, *Mater. Res. Bull.*, 1997, **32**, 67–74.

53 D. Ghosh, U. Dutta, A. Haque, N. E. Mordvinova, O. I. Lebedev, K. Pal, A. Gayen, P. Mahata, A. K. Kundu and M. Motin Seikh, Evidence of low temperature spin glass transition in bixbyite type FeMnO3, *Mater. Sci. Eng., B*, 2017, **226**, 206–210, DOI: 10.1016/j.mseb.2017.09.022.

54 S. Middey, S. Ray, K. Mukherjee, P. L. Paulose, E. V Sampathkumaran, C. Meneghini, S. D. Kaushik, V. Siruguri, K. Kovnir and D. D. Sarma, Glasslike ordering and spatial inhomogeneity of magnetic structure in Ba 3 FeRu 2 O 9: role of Fe/Ru site disorder, *Phys. Rev. B*, 2011, **83**, 144419.

55 R. M'nassri, N. Chniba-Boudjada and A. Cheikhrouhou, 3D-Ising ferromagnetic characteristics and magnetocaloric study in Pr0.4Eu0.2Sr0.4MnO3 manganite, *J. Alloys Compd.*, 2015, **640**, 183–192, DOI: 10.1016/j.jallcom.2015.03.220.

56 S. K. Çetin, M. Acet, M. Güneş, A. Ekicibil and M. Farle, Magnetocaloric effect in (La1−xSmx)0.67Pb0.33MnO3 (0 ≤ x ≤ 0.3) manganites near room temperature, *J. Alloys Compd.*, 2015, **650**, 285–294, DOI: 10.1016/j.jallcom.2015.07.217.